

---

# Quantitation of Pulmonary Transgene Expression with PET Imaging

Jean-Christophe Richard, MD<sup>1</sup>; Zhaohui Zhou, MD<sup>1</sup>; Delphine L. Chen, MD<sup>1</sup>; Mark A. Mintun, MD<sup>1</sup>; David Piwnica-Worms, MD, PhD<sup>1</sup>; Phillip Factor, MD<sup>2</sup>; Datta E. Ponde, PhD<sup>1</sup>; and Daniel P. Schuster, MD<sup>1</sup>

<sup>1</sup>Washington University School of Medicine, St. Louis, Missouri; and <sup>2</sup>Columbia University College of Physicians and Surgeons, New York, New York

---

PET imaging represents a promising approach for noninvasive monitoring of reporter gene expression in living subjects. We evaluated the relationship between various methods of quantifying the imaging signal and in vitro assays of the expression of a PET reporter gene (a mutant *Herpes simplex virus-1* thymidine kinase (mHSV1-*tk*); 9-(4-<sup>18</sup>F-fluoro-3-hydroxymethylbutyl)guanine (<sup>18</sup>F-FHBG) was used as the PET reporter probe. **Methods:** In 14 rats, pulmonary gene transfer was performed by intratracheal administration of various amounts of an adenovector containing a fusion gene encoding for mHSV1-*tk* and an enhanced green fluorescent protein. Three days later, the animals were divided into 2 groups. One group ( $n = 7$ ) did not receive any other interventions. The other group was treated with  $\alpha$ -naphthylthiourea (ANTU) to increase pulmonary vascular permeability. All rats were injected intravenously with <sup>18</sup>F-FHBG. Two additional rats in both groups received a null adenovector and served as controls. In the normal rats, repetitive blood samples were obtained and PET imaging was performed simultaneously using a dynamic imaging protocol. Rate constants estimating <sup>18</sup>F-FHBG transport ( $K_1$ ) or trapping ( $k_3$ ) within target cells were generated by compartmental modeling. After euthanasia, pulmonary uptake of <sup>18</sup>F-FHBG was determined using a  $\gamma$ -counter in all rats, and in vitro assays of transgene expression were performed on lung tissue. **Results:** In normal rats, pulmonary uptake of <sup>18</sup>F-FHBG increased as thymidine kinase (TK) activity increased only at low levels of mHSV1-*tk* expression and then plateaued as TK activity continued to increase. Compartmental modeling failed to improve the correlation with in vitro assays of transgene expression. However, a linear relationship was obtained between the pulmonary uptake of <sup>18</sup>F-FHBG and in vitro assays of TK activity in rats treated with ANTU. **Conclusion:** In rodent lungs, <sup>18</sup>F-FHBG uptake appears to be a function of both transport into tissues expressing the transgene as well as the level of transgene expression itself.

**Key Words:** PET; compartmental modeling; herpes simplex virus-1 thymidine kinase; 9-(4-<sup>18</sup>F-fluoro-3-hydroxymethylbutyl)guanine; reporter gene

**J Nucl Med 2004; 45:644–654**

**R**ecent studies indicate that PET may be a useful imaging tool to monitor reporter transgene expression in vivo (1,2). The basic concept underlying the imaging strategy is that a reporter transgene (PET reporter gene) capable of trapping or binding a suitable positron-emitting radionuclide-labeled tracer (PET reporter probe) is introduced into a target tissue via a suitable vector. After PET reporter probe administration, a PET imaging signal is generated as the PET reporter probe accumulates over time within tissues expressing the PET reporter transgene.

As these techniques have developed over the past decade, several different PET reporter genes have been described, encoding for intracellular enzymes (3–5), membrane-bound receptors (6), or cell-membrane transporters (7). Of these, wild-type (3) and mutant variants (8–10) of the *Herpes simplex virus-1* thymidine kinase (HSV1-*tk*) have received the most attention because they are not naturally expressed in mammalian cells and they have the theoretic advantage of allowing signal amplification compared with nonenzyme-based strategies (each reporter protein metabolizes several molecules of radioactive probe), thereby improving sensitivity (11,12). Various PET reporter probes have also been developed, including several with relative substrate specificity for different HSV1-*tk* mutants (mHSV1-*tk*) (8,10). To date, however, the optimal combination of PET reporter transgene and probe is still controversial (13,14).

Previous mutagenesis and screening studies identified mutant forms of HSV1-*tk* with enhanced selectivity and affinity for acycloguanosine derivatives (15). Thus, to image mutant HSV1-*tk*, radiolabeled analogs, such as the acycloguanosine derivative 9-(4-<sup>18</sup>F-fluoro-3-hydroxymethylbutyl)guanine (<sup>18</sup>F-FHBG), show improved sensitivity and rapid blood clearance, thereby reducing background and improving the signal-to-noise ratio (16). A key premise underlying the use of PET imaging to monitor and quantify transgene expression is that, over a relevant physiologic range, the expression level of the reporter gene is directly related to the PET imaging signal, which in turn depends on the tissue accumulation of the PET reporter probe (16,17).

However, although several studies have confirmed the sensitivity of the <sup>18</sup>F-FHBG/mHSV1-*tk* PET reporter com-

---

Received Oct. 20, 2003; revision accepted Dec. 2, 2003.

For correspondence or reprints contact: Daniel P. Schuster, MD, University Box 8225, Washington University School of Medicine, 660 S. Euclid Ave., St. Louis, MO 63110.

E-mail: schusted@msnotes.wustl.edu

ination (14,18), the strength of the correlation between tissue  $^{18}\text{F}$ -FHBG uptake and tissue-based assays of reporter gene expression has been variable (18,19). Indeed, several studies seem to suggest that the imaging signal may plateau as high levels of mHSV1-*tk* are achieved in target tissue (18,19).

In this study, we evaluated, in rodent lungs, the correlation between the pulmonary uptake of  $^{18}\text{F}$ -FHBG and corresponding in vitro assays when high expression levels of mHSV1-*tk* were achieved. The results suggest that in vivo pulmonary uptake of the radiotracer is a function of both reporter gene expression and tracer transport into lung tissue.

## MATERIALS AND METHODS

The present study was approved by the Washington University School of Medicine's Animal Studies Committee.

### Adenovectors

Replication-deficient (E1a/E3 deleted) recombinant human type 5 adenoviruses (Ad-CMV-mNLS-HSV1sr39tk-*egfp*) containing a fusion gene encoding for a mutant *Herpes simplex virus* type-1 thymidine kinase (mNLS-HSV1sr39tk (9)) and an enhanced green fluorescent protein (*egfp*), under the control of a constitutive cytomegalovirus (CMV) promoter, were constructed and purified as described elsewhere (18). A control vector (Ad-CMVnull) was constructed with a shuttle vector containing no complementary DNA.

### Radiotracer Synthesis

$^{18}\text{F}$ -FHBG was synthesized, as previously described, using a microwave-mediated method to generate high chemical yield and purity (20), with specific activity ranging between 70 and 110 GBq/mmol.

### Experimental Protocol

An initial study was performed on 9 normal Sprague-Dawley rats (mean weight  $\pm$  SD,  $257 \pm 46$  g). Seven rats were intratracheally infected with various amounts of Ad-CMV-mNLS-HSV1sr39tk-*egfp* ( $5 \times 10^9$  to  $5 \times 10^{10}$  viral particles [VP]) to induce a wide range of mNLS-HSV1sr39tk expression in the lungs. Two additional rats were infected with the control vector. PET and other measurements were obtained 3 d after pulmonary gene transfer.

Nine additional Sprague-Dawley rats (mean weight  $\pm$  SD,  $357 \pm 56$  g) were studied to test the influence of  $\alpha$ -naphthylthiourea (ANTU)-induced changes in pulmonary vascular permeability on  $^{18}\text{F}$ -FHBG uptake within the lungs. Seven animals were intratracheally infected with Ad-CMV-mNLS-HSV1sr39tk-*egfp* at doses that matched the viral doses used in the normal rats ( $5 \times 10^9$  to  $5 \times 10^{10}$  VP). Similarly, 2 additional rats were infected with the control vector. Three days after pulmonary gene transfer, 2 mL/kg body weight of ANTU were injected intraperitoneally. After an additional 2.5 h, the animals were injected intravenously with  $19.4 \pm 3.3$  kBq/g of body weight of  $^{18}\text{F}$ -FHBG and euthanized 75 min after tracer injection.

Adenovirus delivery to rat lungs was performed using a surfactant-based method as previously described (18,21).

## PET Studies

Animals were anesthetized with isoflurane before surgical insertion of arterial and venous catheters into the carotid artery and jugular vein, respectively. Animals were then placed in the supine position within the microPET scanner.

Dynamic PET imaging was performed in the normal rats on a microPET-R4 camera (22). Images were obtained serially over a period of 78 min using the following imaging protocol: 16 images of 10-s duration each, 6 images of 30 s, 1 image of 2 min, and 14 images of 5 min (total of 37 frames). PET imaging and tracer injection (over 30 s) were begun simultaneously. The mean injected dose  $\pm$  SD of  $^{18}\text{F}$ -FHBG was  $46 \pm 7$  kBq/g of body weight.

Beginning with tracer injection, approximately 5  $\mu\text{L}$  of arterial blood were withdrawn every 8 s during the first 2 min using disposable capillary tubes (Wiretrol II; Drummond Scientific Co.), and the intervals between withdrawal were progressively increased to every 5 min until the end of experiment. The radioactivity in these samples was measured in a  $\gamma$ -counter, previously cross-calibrated with the microPET device. Counts in each sample were corrected for counting efficiency and radioactive decay (to the time of tracer injection), normalized for sample weight, and expressed as kilobecquerels per milliliter, assuming a density for blood of 1.05. Blood time-activity curves were then linearly interpolated to match the time of PET image acquisition.

### Image Analysis

On multiple transverse slices of the PET images, regions of interest (ROIs) were drawn on the left and right lungs using Analyze version 4.0 for image analysis (23) and subsequently merged to obtain a measurement of pulmonary radioactivity originating from the whole lung volume. Radioactivity measurements were then decay corrected to the time of tracer injection and pulmonary time-activity curves were generated from the multiple-image dataset (Fig. 1).

### Data Analysis

Three forms of quantitation were used to evaluate the uptake of  $^{18}\text{F}$ -FHBG by the lungs.

*Percentage of Injected Dose per Milliliter of Lung.* Pulmonary radioactivity assessed with PET imaging was averaged for the final 4 imaging frames and normalized to the injected dose (ID) of  $^{18}\text{F}$ -FHBG. This value represented the %ID/mL of lung, as measured from 58 to 78 min after tracer injection.

*Patlak Graphical Analysis.* The Patlak influx constant (Patlak  $K_i$ ) (24,25) was obtained by fitting the experimental data points obtained after tracer equilibration to the following linear equation:

$$\frac{C_T(t)}{C_A(t)} = \text{Patlak } K_i \times \frac{\int_0^t C_A(\tau) d\tau}{C_A(t)} + B, \quad \text{Eq. 1}$$

where  $C_T(t)$  and  $C_A(t)$  are, respectively, tissue and blood radioactivity at each sample time point ( $t$ ),  $\tau$  is the integration variable,  $K_i$  is the Patlak influx constant, and  $B$  is a parameter representing the initial volume of distribution of the tracer (the intercept when plotted graphically). The initial point in the linear regression was chosen based on visual inspection of the data ( $6 \pm 2$  min after tracer injection for all animals). The average correlation of determination ( $R^2$ ) was  $0.91 \pm 0.19$  for all animals.  $K_i$  was calculated from the slope of the equation generated by the regression.

*3-Compartmental Model.* The kinetics of  $^{18}\text{F}$ -FHBG in the lungs were analyzed using a standard 3-compartment model (Fig. 2).

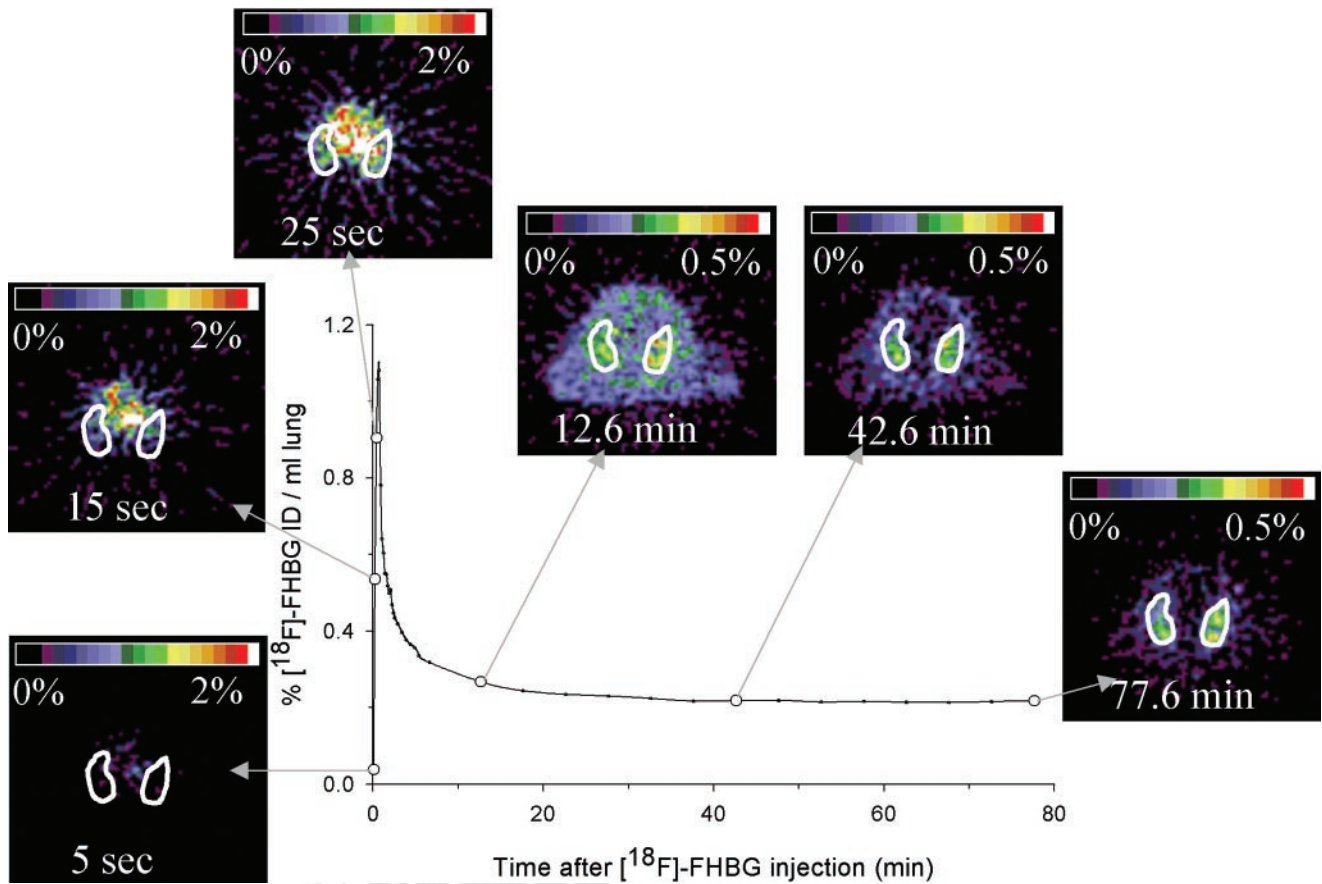


**FIGURE 1.** Generation of pulmonary time-activity curve from multiple-image dataset from 1 experimental animal. Pulmonary ROIs are drawn on multiple transverse slices of PET image and subsequently merged to obtain measurement of pulmonary radioactivity originating from whole lung volume at time of PET image data acquisition. These ROIs are then superimposed on images obtained at each sampling time with PET, to generate lung time-activity curve. For clarity, only 1 of multiple transverse thoracic slices is displayed at 6 of 37 time points. Color scale is shown on top of each PET image and expressed as percentage of  $^{18}\text{F}$ -FHBG injected dose. ID = injected dose.

Model parameters were obtained by fitting the experimental data points to the following equation:

$$C_T(t) = \frac{K_1}{\alpha_2 - \alpha_1} \times [(k_3 + k_4 - \alpha_1)e^{-\alpha_1 t} + (\alpha_2 - k_3 - k_4)e^{-\alpha_2 t}] \otimes C_A(t) + \text{BVC}_A(t), \quad \text{Eq. 2}$$

where

$\alpha_{2,1} = \frac{1}{2}(k_2 + k_3 + k_4 \pm \sqrt{(k_2 + k_3 + k_4)^2 - 4k_2k_4})$ ;  $\otimes$  is the convolution operator; BV is the blood volume component;

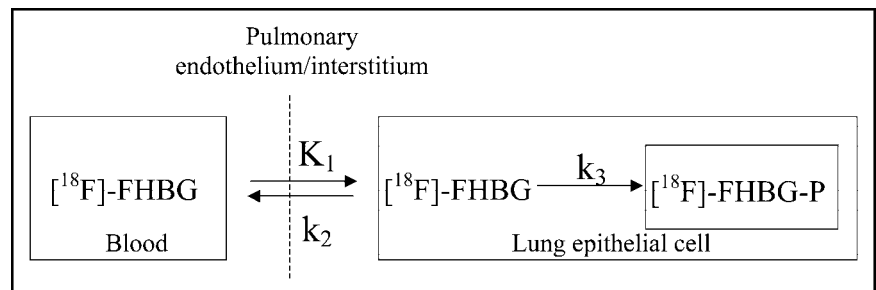
and  $K_1$ ,  $k_2$ ,  $k_3$ , and  $k_4$  represent the individual rate constants (Fig. 2).

Since  $^{18}\text{F}$ -FHBG is assumed to be trapped in cells after phosphorylation by the viral thymidine kinase,  $k_4$  was set to 0 and dropped from the equation.  $K_1$ ,  $k_2$ ,  $k_3$ , and BV were then estimated by non-linear regression using 0.04, 0.04, 0.03, and 0.5 as initial estimates.

The influx constant (CM  $K_1$ ) was then calculated as:

$$\text{CM } K_1 (\text{mL blood/mL lung/min}) = K_1 \frac{k_3}{(k_2 + k_3)}. \quad \text{Eq. 3}$$

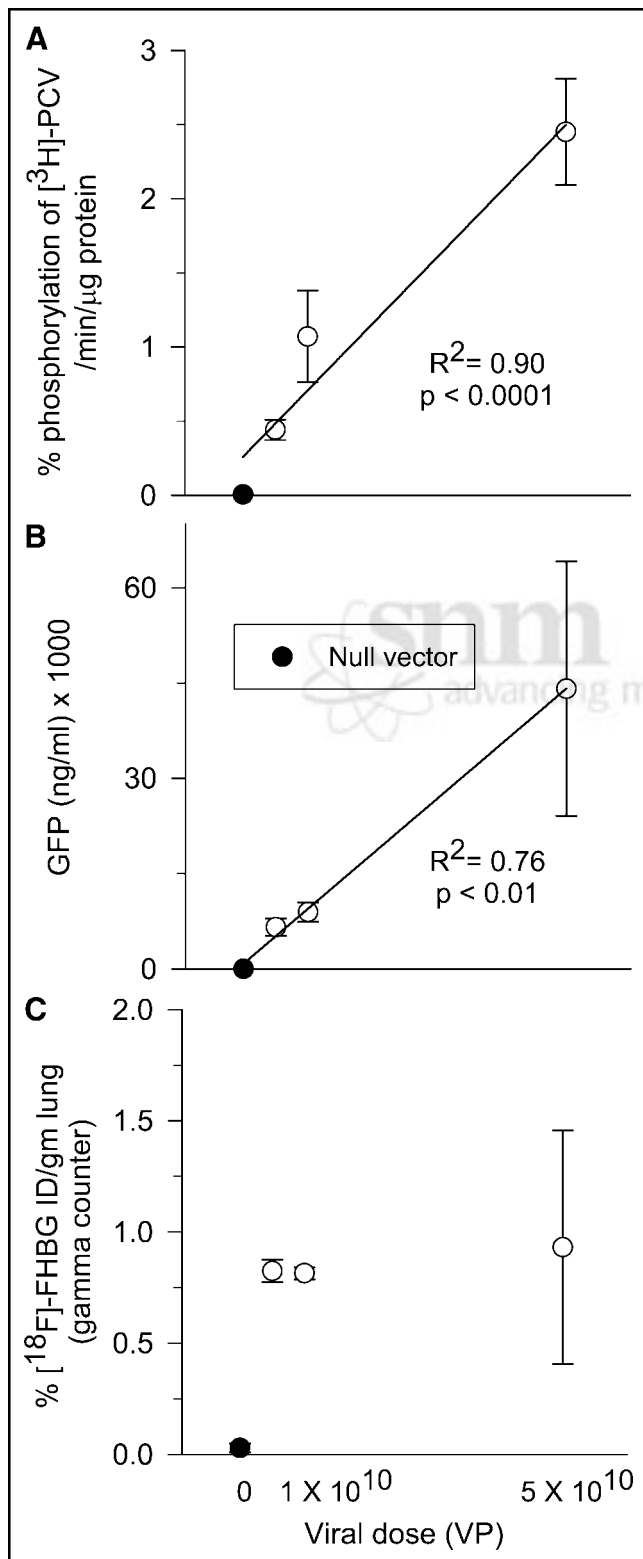
**FIGURE 2.** Diagram of 3-compartment model representing  $^{18}\text{F}$ -FHBG kinetics within lungs. In this model,  $K_1$  and  $k_2$  are rate constants representing transport of  $^{18}\text{F}$ -FHBG into and out of cells, and  $k_3$  represents rate of phosphorylation of  $^{18}\text{F}$ -FHBG in cells expressing viral TK. Since  $^{18}\text{F}$ -FHBG-P is assumed to be trapped intracellularly,  $k_4$  (rate constant representing  $^{18}\text{F}$ -FHBG dephosphorylation) was not included in model.



### Ex Vivo Assessment of Pulmonary Radioactivity with $\gamma$ -Counting

Immediately after completion of PET imaging, rats were deeply anesthetized by an overdose of ketamine and xylazine. After thoracotomy, the lung circulation was perfused with 0.9% saline

via the spontaneously beating right ventricle. The lungs were then harvested and radioactivity of the whole lung was measured in the  $\gamma$ -counter that was used to count radioactivity in the blood samples. Lung activity values were corrected for counting efficiency and radioactive decay (to the time of tracer injection) and normalized to the  $^{18}\text{F}$ -FHBG ID. The result was then expressed as %ID/g of lung.



### Ex Vivo Quantitation of Reporter Gene Expression in Normal Rats

After euthanasia and the determination of pulmonary radioactivity with  $\gamma$ -counting, tissue samples were assayed for the 2 adenovector gene products, thymidine kinase (TK) and enhanced green fluorescent protein (eGFP). TK enzyme activity in lung tissue extracts was assessed on 1  $\mu\text{g}$  of protein, as previously described (18,26). Briefly, 8- $^3\text{H}$ -penciclovir was added to the preparation, and its phosphorylated compound was quantified in an anion-exchanger filter using a  $\beta$ -counter. Results were then expressed as a percentage of 8- $^3\text{H}$ -penciclovir phosphorylation per min/ $\mu\text{g}$  of protein. Enhanced eGFP levels in lung tissue extracts were also quantified using an enzyme-linked immunosorbent assay (ELISA) as previously described (18).

### Statistical Analysis

Linear regression analyses were performed by the least-squares method, using SigmaPlot (SPSS Inc.). Nonlinear regression analyses were performed using the Levenberg–Marquardt optimization method. Goodness of fits were assessed with the coefficient of determination  $R^2$  for linear regression and by plotting residuals for nonlinear regression. The level of statistical significance was set at  $P \leq 0.05$ .

### RESULTS

The relationship between adenoviral dose and several methods of quantifying reporter gene expression are presented in Figure 3. In vitro assays of mutant *Herpes simplex* virus-1 thymidine kinase (mHSV1-TK) activity and eGFP expression (the 2 products of the fusion reporter gene) were both linearly correlated with viral dose ( $P < 0.01$ ; Figs. 3A and 3B). Likewise, there was an excellent correlation of mHSV1-TK activity versus eGFP expression levels by ELISA ( $R^2 = 0.84$ ; data not shown). In contrast, although the pulmonary uptake of  $^{18}\text{F}$ -FHBG was greater at all doses of viral vector than that in rats administered null vector, there was also no correlation between uptake and adenoviral dose (Fig. 3C), nor was there any significant correlation of  $^{18}\text{F}$ -FHBG uptake versus mHSV1-TK activity ( $R^2 = 0.29$ ).

**FIGURE 3.** Quantitation of mHSV1-TK enzyme activity (A), eGFP levels (B), and  $^{18}\text{F}$ -FHBG lung uptake (C) as function of viral dose in 9 rats without lung injury. ○, Mean values at each of viral doses of Ad-CMV-mNLS-HSV1sr39tk-egfp ( $5 \times 10^9$  VP [ $n = 2$  rats],  $1 \times 10^{10}$  VP [ $n = 2$  rats],  $5 \times 10^{10}$  VP [ $n = 3$  rats]). ●, Mean values measured in control animals ( $n = 2$ ). Bars are SDs. Linear regression was performed on data points from all rats and corresponding regression line is displayed when slope was statistically significant compared with slope of zero. PCV = penciclovir.

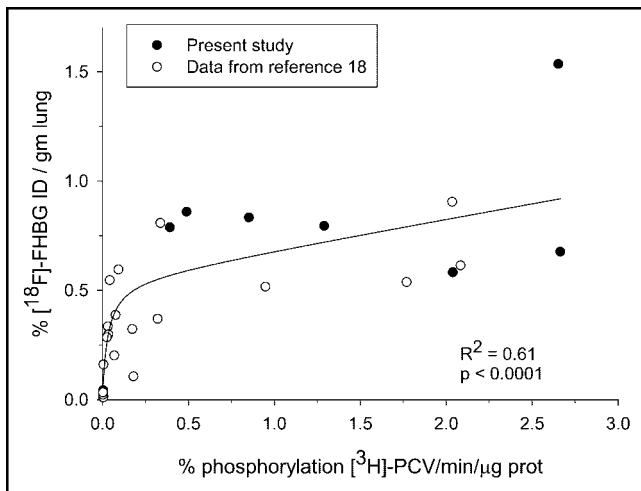


**FIGURE 4.** Relationship between lung uptake of  $^{18}\text{F}$ -FHBG and mHSV1-TK enzyme activity in 28 rats. Results of 9 rats of this study without lung injury (●) are combined with data of 19 rats from previous study of our group (○) (18). Data were fitted to a hyperbolic equation, and corresponding regression curve and  $R^2$  are displayed. PCV = penciclovir.

Figure 4 combines data from the current study with similar data from a previous study that reported a linear correlation between  $^{18}\text{F}$ -FHBG uptake and mHSV1-TK activity (18).  $^{18}\text{F}$ -FHBG uptake increases rapidly at low levels of reporter gene expression (assayed as thymidine kinase activity) but then plateaus and essentially remains steady as mHSV1-*tk* expression increases.

The accuracy of pulmonary  $^{18}\text{F}$ -FHBG tissue radioactivity in lung ROIs on the PET images was assessed with correlations to  $\gamma$ -counter radioactivity measurements obtained on ex vivo lung samples ( $R^2 = 0.98$ ; data not shown). The slope of the relationship was 0.28, comparable to that previously reported in a similar comparison (18). A slope less than unity likely represents the lack of correction for lung density on the imaging measurements, given that attenuation corrections have not yet been incorporated into microPET image reconstruction algorithms (the PET data are expressed as per milliliter lung, whereas the  $\gamma$ -counter data are expressed as per gram lung; normal lung density is 0.3–0.4 g/mL lung in rats (27)).

The clearance of  $^{18}\text{F}$ -FHBG from blood, based on direct blood sampling and expressed as the mean  $\pm$  SD for all animals in this study, is shown in Figure 5. After a peak in blood radioactivity after tracer injection, a biphasic decrease was observed with a complex first phase followed by a monoexponential slower phase beginning 30 min after tracer injection (mean half-life  $\pm$  SD,  $31 \pm 4$  min). At the end of the experiment, blood radioactivity levels were nearly 2 orders of magnitude lower than the measured peak value and showed only minimal variability among experimental animals ( $^{18}\text{F}$ -FHBG  $0.04 \pm 0.01$  %ID/g blood [mean  $\pm$  SD]).

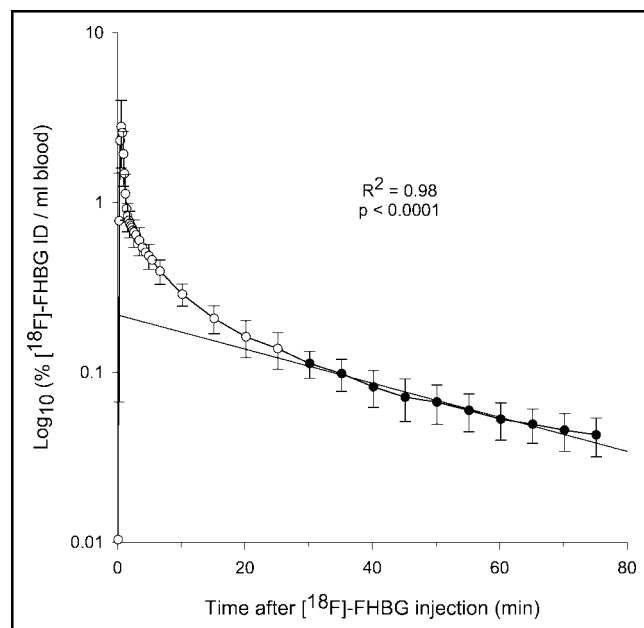
Examples of fitted lung time–activity curves using the 3-compartment model (Fig. 2 and Eq. 2) are shown in

Figure 6 for 2 representative animals. Figures 6A and 6B were obtained from an animal infected with Ad-CMV-mNLS-HSV1*sr39tk-egfp* and in a control animal infected with the null vector, respectively. Plotting of residuals over time (Figs. 6C and 6D), used as an estimate of goodness of fit (28), showed a random distribution of residuals about 0 in all animals of the study.

Patlak plots also showed excellent linearity by linear regression analysis for all animals (Fig. 7). The mean  $\pm$  SD for the coefficient of determination,  $R^2$ , was  $0.999 \pm 0.001$  for Ad-CMV-mNLS-HSV1*sr39tk-egfp*-infected animals and  $0.58 \pm 0.09$  for the 2 control animals.

Overall, estimates of the influx constant,  $K_i$ , by compartmental modeling and by Patlak analysis were strongly and linearly correlated ( $R^2 = 1$ ,  $P \leq 0.0001$ ; data not shown). A similar linear correlation was observed between the influx constant obtained by compartmental modeling and  $^{18}\text{F}$ -FHBG %ID ( $R^2 = 0.94$ ,  $P \leq 0.0001$ ).

No relationship between either the net uptake of tracer (quantified as the slope of the Patlak relationship) or  $k_3$  (the rate constant presumed to represent “trapping” of tracer within tissues expressing the *tk* reporter gene) could be identified with the assay of TK activity (as an in vitro index of reporter gene expression (Fig. 8)). This lack of correlation cannot be attributed to poor data quality given the results presented in Figures 5–7. Note once again, however, that values obtained in all rats infected with the adenovector carrying the reporter gene were consistently higher than



**FIGURE 5.** Blood pharmacokinetics of  $^{18}\text{F}$ -FHBG. Data points are average values of blood radioactivity for 9 rats of study and bars are SDs. ○, Data points collected during first 30 min. ●, Subsequent data points fitted with monoexponential equation. Corresponding regression line coefficients of determination  $R^2$  are displayed. For clarity, some SD bars were omitted.

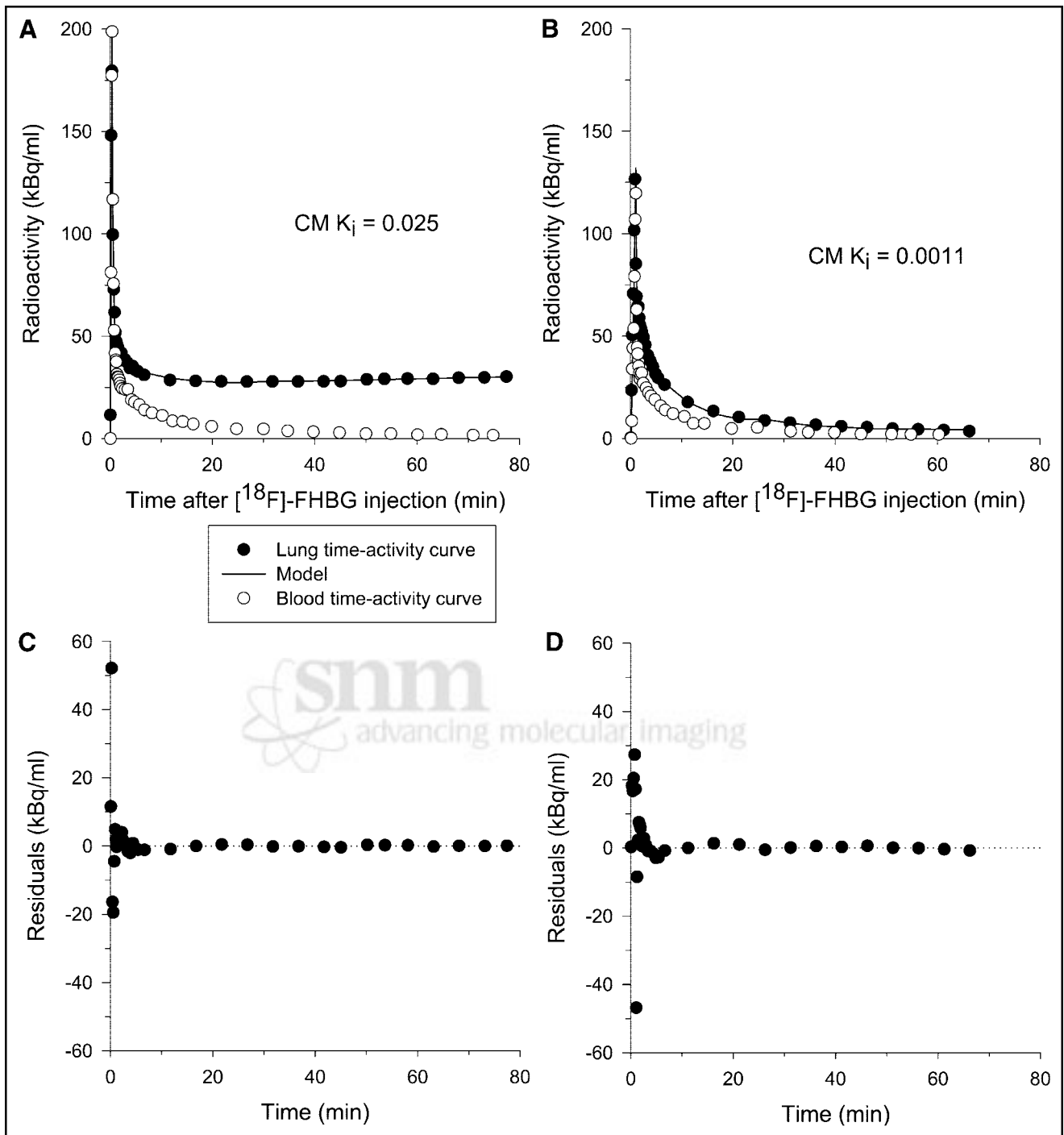


**FIGURE 6.** Examples of curve fitting using compartmental modeling obtained in 2 rats infected with Ad-CMV-mNLS-HSV1sr39tk-egfp (A) and with null vector (B), respectively. Blood (○) and lung (●) time-activity curves are displayed. Continuous line represents fitted lung data points using 3-compartment model shown in Figure 2. (C and D) Corresponding plots of residuals over time from regression analysis.  $CM K_i$  = influx constant calculated from individual rate constants shown in Figure 2 (see Eq. 3); BV = blood volume expressed as percentage of ROI volume.

values obtained in the rats infected with the null vector (Fig. 8; Table 1).

In rats treated with ANTU, levels of reporter gene expression (assessed with in vitro assays) were not significantly different than those in the normal rats ( $1.38\% \pm$

$0.95\%$  vs.  $1.29\% \pm 0.39\%$   $^3\text{H}$ -penciclovir phosphorylation per min/ $\mu\text{g}$  protein). However, in contrast to normal rats (Fig. 4),  $^{18}\text{F}$ -FHBG uptake was linearly correlated with in vitro assays of TK activity (Fig. 9A;  $R^2 = 0.56$ ,  $P < 0.05$ ). Furthermore, total lung uptake (expressed as %ID in the

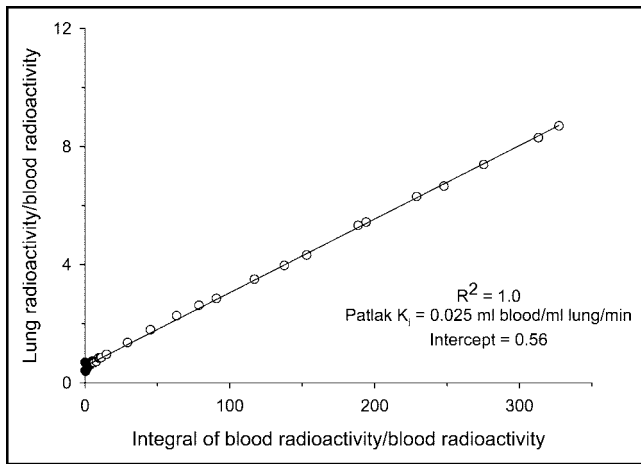


**FIGURE 7.** Patlak graphical analysis of  $^{18}\text{F}$ -FHBG pulmonary kinetics in rat whose compartmental modeling fits are presented in Figure 6A. Animal was infected with Ad-CMV-mNLS-HSV1sr39tk-egfp. ●, Early experimental data points on which assumption of curve linearity assumed by model is not satisfied. ○, Experimental data points on which linear regression analysis was performed. Slope ( $K_i$ ), intercept, and coefficient of determination ( $R^2$ ) of straight line fit are displayed.  $K_i$  = Patlak influx constant.

whole lung) was positively correlated with normalized lung weight (as a surrogate for severity of edema due to increased permeability) in the ANTU group (Fig. 9B) but not in the normal rats (Fig. 9C). The level of mHSV1-*tk* gene expression, on the other hand, achieved in the ANTU group (assessed with in vitro assays) did not correlate with normalized lung weight ( $R^2 = 0.25$ ,  $P > 0.05$ ; data not shown), demonstrating that these were likely independent factors determining the uptake of  $^{18}\text{F}$ -FHBG in the lung.

## DISCUSSION

The main finding of this study is that lung tissue accumulation of the PET reporter probe  $^{18}\text{F}$ -FHBG is not linearly related to the tissue expression of the mutant PET reporter gene HSV1-*tk* over the full range of transgene expression obtained in lung tissue. In addition, our results appear to indicate that it is the pulmonary endothelium that may be acting as the potentially critical barrier, limiting access of the tracer to target cells expressing the viral thymidine kinase.

These results appear to contradict the results of several other studies that sought to validate image quantitation of gene expression against in vitro assays of HSV1-TK activity. For instance, highly linear correlations have been reported between in vitro assays of gene expression and the tissue accumulation of both pyrimidine (such as 2'-fluoro-2'-deoxy-1- $\beta$ -D-arabinofuranosyl-5-iodouracil [FIAU]) and acycloguanosine derivatives (such as the  $^{18}\text{F}$ -FHBG used in the current study) (2,29).

More recently, several studies have noted a possible plateauing of tracer uptake as tissue measurements of

HSV1-TK activity (the in vitro measure of gene expression) increased (18,19,30). However, the low number of experimental points and the relatively limited range of transgene expression in these studies precluded any definite conclusions. For instance, using a closely related PET reporter gene and the identical PET reporter probe as used in the current study, the upper limit of TK activity was 0.5%  $^3\text{H}$ -penciclovir phosphorylation per min/ $\mu\text{g}$  protein in 2 previous reports (19,31) (compared with 6-fold higher levels in this study; Figs. 4 and 9).

Our study addresses these issues in several ways. First, we combined the results of the present study with those of a previous study by our group using identical experimental protocols (Fig. 4) (18). Second, as just noted, we were able to achieve a wide range of tissue gene expression, measured as TK activity in vitro. Third, the scattergram shown in Figure 4 is the largest ( $n = 28$ ) single comparison of tissue accumulation of a PET reporter probe versus an in vitro

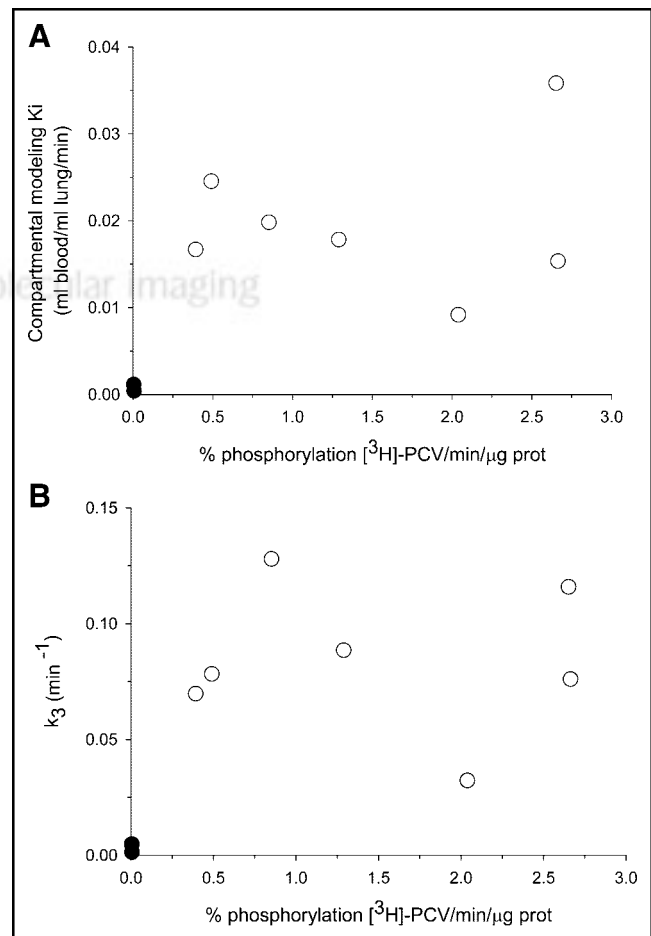


**FIGURE 8.** Relationships between mHSV1-TK enzyme activity assessed in vitro and compartmental modeling results (using 3-compartment model shown in Fig. 2). ○, Data points obtained in each individual rat infected with Ad-CMV-mNLS-HSV1sr39tk-egfp ( $n = 7$ ). ●, Data points obtained in 2 animals infected with control virus ( $n = 2$ ).  $K_i$  (influx constant) represents net uptake of tracer into irreversibly bound compartment.  $K_i$  and  $k_3$  are individual rate constants shown in Figure 2. PCV = penciclovir.

**TABLE 1**  
Computed Rate Constants Describing  $^{18}\text{F}$ -FHBG Kinetics (Based on Model in Figure 2)

Rats	$K_1$	$k_2$	$k_3$	$K_i$
mHSV1- <i>tk</i> ( $n = 7$ )	$0.069 \pm 0.026$	$0.222 \pm 0.139^*$	$0.084 \pm 0.031^*$	$0.199 \pm 0.008^*$
Control (null vector) ( $n = 2$ )	$0.123^\dagger$	$0.508 \pm 0.741$	$0.005 \pm 0.001$	$0.001 \pm 0.000$

\* $P < 0.05$  compared with data from null vector rats.  
 $^\dagger n = 1$  only; estimate of  $K_1$  in 1 rat was unreliable.

assay of gene expression. Note that in Figure 4, the plateau effect only occurs above TK activity levels of 0.5%  $^3\text{H}$ -penciclovir phosphorylation per min/g protein.

Several factors might account for this apparent plateau effect. Competition for phosphorylation between  $^{18}\text{F}$ -FHBG and cellular thymidine is one possibility, as recently noted by Min et al. (14). However, for this to have been a factor here, thymidine concentrations would have to have increased as a function of increasing expression of the transgene; there is no reason to believe that this was the case.

Another possible cause is that tracer availability to the viral transgene was restricted in some way. For instance,  $^{18}\text{F}$ -FHBG was shown recently to accumulate much more slowly in mammalian cells expressing the wild-type HSV1-TK in vitro than other radiolabeled pyrimidine nucleoside derivatives (13), and it was hypothesized that  $^{18}\text{F}$ -FHBG uptake might be limited by cell membrane transport (13). However, the mechanisms contributing to the final levels of radiolabeled probe uptake are complex. For example, pyrimidine nucleoside derivatives (i.e., FIAU) show

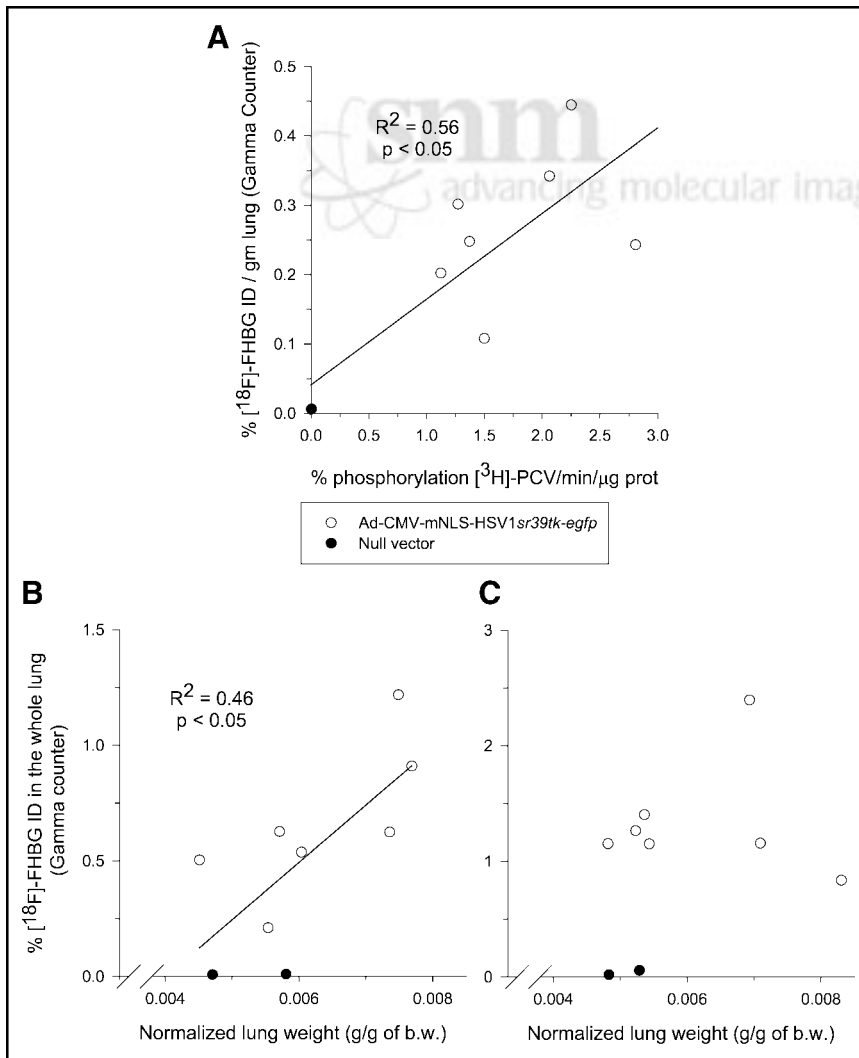


**FIGURE 9.** Quantitation of reporter gene expression during permeability edema. (A) Relationship between lung uptake of  $^{18}\text{F}$ -FHBG and mHSV1-TK enzyme activity in 9 rats with ANTU-induced increase in pulmonary vascular permeability. (B and C) Relationship between total lung uptake (expressed as %ID in whole lung) and normalized lung weight in 9 rats with ANTU-induced increases in pulmonary vascular permeability (B) and in 9 normal rats (C). ○, Data points obtained in rats infected with Ad-CMV-mNLS-HSV1sr39tk-egfp. ●, Data points obtained in animals infected with control virus. Regression line is displayed when significant linear correlation was obtained. PCV = penciclovir; b.w. = body weight.

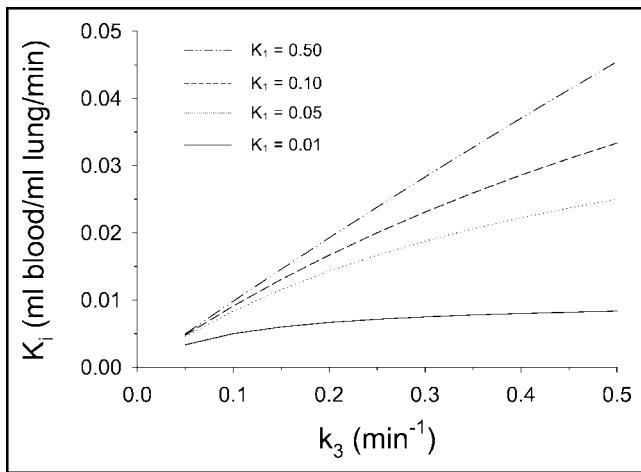


**FIGURE 10.** Simulation of effect of increasing  $K_1$  on relationship between  $K_1$  and  $k_3$  when ratio of  $K_1/k_2$  is kept constant, based on model shown in Figure 2.

higher cross-reactivity with endogenous TK than acycloguanosine derivatives (such as FHBG), and standard cell assays to determine levels of trapped radiolabeled nucleotides will not distinguish between product arising from the 2 different enzymes. Furthermore, pyrimidine and acycloguanosine derivatives have different affinities for known nucleoside transporters. Thus, whole cell assays cannot differentiate the effects of transport from enzyme efficiency.

To isolate different factors potentially involved in limiting pulmonary  $^{18}\text{F}$ -FHBG uptake despite evidence for increasing levels of gene expression, we analyzed the tissue and blood time-activity data with a standard 3-compartmental model that assumes both a transport step into target cells and a trapping (phosphorylation) step (Fig. 2). However, neither the net uptake of tracer ( $K_1$ ) nor trapping per se (estimated by the rate constant  $k_3$ ) correlated with the in vitro assay of gene expression (Fig. 8).

This absence of a significant correlation between  $k_3$  and an independent measurement of the underlying physiologic process it allegedly represents calls into question the validity of the standard 3-compartment model assumed to describe pulmonary  $^{18}\text{F}$ -FHBG kinetics. We thus hypothesized that the model identified in Figure 2 was too simple and that, though transport into target cells per se might not be rate limiting, transport into the immediate extracellular environment of these tissues might be. For instance, the viral vector is administered intratracheally, resulting primarily in alve-

olar epithelial cell infection and gene transfer. However, the PET reporter probe is administered intravenously. It must therefore cross pulmonary vascular endothelial and interstitial compartments before it can gain access to alveolar epithelial cells. Trapping of tracer that makes it to this point might indeed be a function of transgene expression (i.e., “ $k_3$ ”), but overall uptake might be limited by the barrier posed by the endothelium-interstitium.

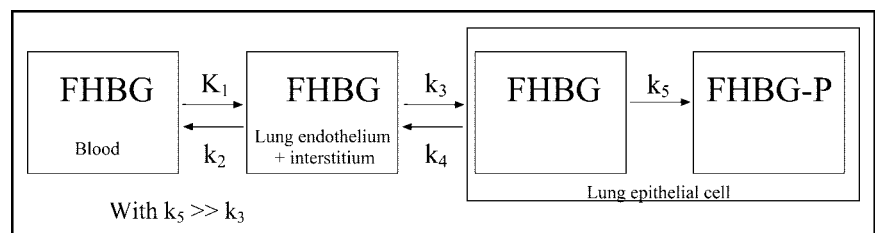
To test this possibility, we used a low dose of the thiourea ANTU to increase the permeability of the pulmonary endothelial barrier. We used a dose that has been reported to increase vascular permeability with minimal development of pulmonary edema (which itself might interfere with tracer access to infected cells) (32–34). Although such an intervention is hardly precise, we nevertheless observed a linear relationship in ANTU-treated rats between  $^{18}\text{F}$ -FHBG uptake and the in vitro assay of mHSV1-TK activity (Fig. 9A vs. Fig. 4). Furthermore, we also observed a linear correlation between tracer uptake and lung weight (used as a surrogate for severity of change in endothelial permeability) in the ANTU-treated rats but not in the normal rats (Fig. 9B vs. Fig. 9C).

As it turns out, the fact that  $K_1$  (the transport step) can limit net uptake of tracer ( $K_1$ ), despite increasing levels of an enzyme that is designed to trap the tracer, is entirely consistent with the standard 3-compartment model. To illustrate this point, Figure 10 shows a simple simulation in which  $K_1$  was plotted against  $k_3$  for different values of  $K_1$  (where the ratio of  $K_1/k_2$  was kept constant). Note that at low levels of  $K_1$ , net uptake of tracer plateaus despite increasing levels of  $k_3$ .  $K_1$  must be increased by 50-fold before  $K_1$  and  $k_3$  are linearly correlated over the full range of  $k_3$  values in this illustration.

The change in the relationship between pulmonary uptake of  $^{18}\text{F}$ -FHBG and in vitro measures of gene expression after vascular permeability was increased by the administration of ANTU is consistent with an increase in  $K_1$ . The result is a linearization of the relationship (Fig. 9). Accordingly, we speculate that the kinetics of  $^{18}\text{F}$ -FHBG uptake in the lungs are better exemplified by a 4-compartmental model (Fig. 11), in which the second compartment represents the endothelial-interstitial barrier between tracer in the vascular space and tracer in cells expressing the viral kinase.

Since the pulmonary endothelium-interstitium appears to pose a barrier for intravenously administered  $^{18}\text{F}$ -FHBG uptake by pulmonary epithelial cells expressing a reporter

**FIGURE 11.** Revised (4-compartment) model of  $^{18}\text{F}$ -FHBG kinetics within lungs. For definition of rate constants, see Figure 2.



imaging transgene, its possible that inhalational delivery of the radiotracer might improve the correlation between imaging signal and in vitro assays of reporter transgene expression. However, though this strategy might work well in normal lungs, it would be difficult to ensure that all portions of the lungs were equally exposed to radiotracer (a necessary condition if quantitation is to be meaningful) during disease states in which regional ventilation would be expected to vary considerably. Of course, the kinetics of  $^{18}\text{F}$ -FHBG uptake by the lungs after intravenous administration of the radiotracer might be quite different if endothelial cells rather than epithelial cells were transduced by the gene vector.

There are potentially multiple applications for reporter transgene expression imaging in the lungs, but they will depend on appropriate modifications to the vector expression cassette. For instance, it should now be possible to evaluate the transcriptional expression of an endogenous gene within the lungs of transgenic animals (35,36) by using the corresponding promoter/enhancer of the endogenous gene to drive expression of the reporter gene. Alternatively, by linking a therapeutic gene to a PET reporter gene, one should also be able to infer the level of expression of the therapeutic gene from the expression level of the reporter. Such a strategy could be used to monitor gene therapy for lung diseases such as cystic fibrosis. However, a predictable relationship between the imaging signal obtained with PET and the physiologic effect of any therapeutic gene has yet to be demonstrated.

Although the results of this study present a challenge for applying the strategy of monitoring reporter transgene expression with imaging, it would be inappropriate to assume that this result eliminates the potential value of this PET reporter gene/PET reporter probe combination specifically or the value of the concept underlying the use of PET imaging for “gene expression imaging” more generally. Alternative combinations of imaging reporter genes or reporter probes, possibly applied in different tissues, will likely yield different results with respect to in vitro assays of gene expression.

Furthermore, as we have already shown, measures of  $^{18}\text{F}$ -FHBG uptake are extraordinarily sensitive for detecting mHSV1-*tk* expression (18,19). Accordingly, this (and other similar systems) can be used to study both the onset and the duration of gene expression noninvasively, as recently demonstrated (18,19). This combination of mHSV1-*tk* and  $^{18}\text{F}$ -FHBG has also been used effectively to study the intrapulmonary distribution of vector delivery and to compare different vector vehicles (37).

## CONCLUSION

In conclusion, uptake of the reporter probe  $^{18}\text{F}$ -FHBG appears to be a function of both transport into tissues expressing the reporter transgene mHSV1-*tk* as well as the level of transgene expression itself. Whether this specific

combination of reporter gene and reporter probe can be used to monitor a “therapeutic” transgene depends on the level of expression that is required to achieve a physiologic effect. Until such studies are performed, this—as well as several other potential reporter combinations—should continue to be evaluated.

## ACKNOWLEDGMENTS

The authors thank Jim Kozlowski for his technical contributions to this study and gratefully acknowledge the support provided by the microPET facility staff in the Division of Radiologic Sciences of Washington University School of Medicine. This research was supported by National Institutes of Health grants HL32815 and CA94056.

## REFERENCES

1. Tjuvajev JG, Joshi A, Callegari J, et al. A general approach to the non-invasive imaging of transgenes using cis-linked herpes simplex virus thymidine kinase. *Neoplasia*. 1999;1:315–320.
2. Liang Q, Gotts J, Satyamurthy N, et al. Noninvasive, repetitive, quantitative measurement of gene expression from a bicistronic message by positron emission tomography, following gene transfer with adenovirus. *Mol Ther*. 2002;6:73–82.
3. Tjuvajev JG, Stockhammer G, Desai R, et al. Imaging the expression of transfected genes in vivo. *Cancer Res*. 1995;55:6126–6132.
4. Gambhir SS, Barrio JR, Wu L, et al. Imaging of adenoviral-directed herpes simplex virus type 1 thymidine kinase reporter gene expression in mice with radiolabeled ganciclovir. *J Nucl Med*. 1998;39:2003–2011.
5. Haberkorn U, Oberdorfer F, Gebert J, et al. Monitoring gene therapy with cytosine deaminase: in vitro studies using tritiated-5-fluorocytosine. *J Nucl Med*. 1996;37:87–94.
6. MacLaren DC, Gambhir SS, Satyamurthy N, et al. Repetitive, non-invasive imaging of the dopamine D<sub>2</sub> receptor as a reporter gene in living animals. *Gene Ther*. 1999;6:785–791.
7. Groot-Wassink T, Aboagye E, Glaser M, Lemoine N, Vassaux G. Adenovirus biodistribution and noninvasive imaging of gene expression in vivo by positron emission tomography using human sodium iodide symporter as reporter gene. *Hum Gene Ther*. 2002;13:1723–1735.
8. Gambhir SS, Bauer E, Black ME, et al. A mutant herpes simplex virus type 1 thymidine kinase reporter gene shows improved sensitivity for imaging reporter gene expression with positron emission tomography. *Proc Natl Acad Sci USA*. 2000;97:2785–2790.
9. Luker GD, Sharma V, Pica CM, et al. Noninvasive imaging of protein-protein interactions in living animals. *Proc Natl Acad Sci USA*. 2002;99:6961–6966.
10. Ponomarev V, Doubrovin M, Serganova I, et al. Cytoplasmically retargeted HSV1-*tk*/GFP reporter gene mutants for optimization of noninvasive molecular-genetic imaging. *Neoplasia*. 2003;5:245–254.
11. Tjuvajev JG, Chen SH, Joshi A, et al. Imaging adenoviral-mediated herpes virus thymidine kinase gene transfer and expression in vivo. *Cancer Res*. 1999;59:5186–5193.
12. De A, Lewis XZ, Gambhir SS. Noninvasive imaging of lentiviral-mediated reporter gene expression in living mice. *Mol Ther*. 2003;7:681–691.
13. Tjuvajev JG, Doubrovin M, Akhurst T, et al. Comparison of radiolabeled nucleoside probes (FIAU, FHBG, and FHPG) for PET imaging of HSV1-*tk* gene expression. *J Nucl Med*. 2002;43:1072–1083.
14. Min JJ, Iyer M, Gambhir SS. Comparison of [ $^{18}\text{F}$ ]FHBG and [ $^{14}\text{C}$ ]FIAU for imaging of HSV1-*tk* reporter gene expression: adenoviral infection vs stable transfection. *Eur J Nucl Med Mol Imaging*. 2003;30:1547–1560.
15. Black ME, Newcomb TG, Wilson HM, Loeb LA. Creation of drug-specific herpes simplex virus type 1 thymidine kinase mutants for gene therapy. *Proc Natl Acad Sci USA*. 1996;93:3525–3529.
16. Massoud TF, Gambhir SS. Molecular imaging in living subjects: seeing fundamental biological processes in a new light. *Genes Dev*. 2003;17:545–580.
17. Blasberg RG, Tjuvajev JG. Molecular-genetic imaging: current and future perspectives. *J Clin Invest*. 2003;111:1620–1629.
18. Richard JC, Zhou Z, Ponde DE, et al. Imaging pulmonary gene expression with positron emission tomography. *Am J Respir Crit Care Med*. 2003;167:1257–1263.

19. Inubushi M, Wu JC, Gambhir SS, et al. Positron-emission tomography reporter gene expression imaging in rat myocardium. *Circulation*. 2003;107:326–332.
20. Ponde DE, Dence CS, Schuster DP, Welch MJ. Microwave mediated rapid and reproducible radiosynthesis of [<sup>18</sup>F]FHBG. *Nucl Med Biol*. 2004;31:133–138.
21. Factor P, Dumasius V, Saldias F, Brown LA, Sznajder JI. Adenovirus-mediated transfer of an Na<sup>+</sup>/K<sup>+</sup>-ATPase beta subunit gene improves alveolar fluid clearance and survival in hyperoxic rats. *Hum Gene Ther*. 2000;11:2231–2242.
22. Knoess C, Siegel S, Smith A, et al. Performance evaluation of the microPET R4 PET scanner for rodents. *Eur J Nucl Med Mol Imaging*. 2003;30:737–747.
23. Robb R. *Biomedical Imaging: Visualization and Analysis*. New York, NY: John Wiley and Sons; 1999.
24. Patlak CS, Blasberg RG, Fenstermacher JD. Graphical evaluation of blood-to-brain transfer constants from multiple-time uptake data. *J Cereb Blood Flow Metab*. 1983;3:1–7.
25. Patlak CS, Blasberg RG. Graphical evaluation of blood-to-brain transfer constants from multiple-time uptake data: generalizations. *J Cereb Blood Flow Metab*. 1985;5:584–590.
26. Hruba DE, Ball LA. Cell-free synthesis of enzymatically active vaccinia virus thymidine kinase. *Virology*. 1981;113:594–601.
27. Lehnert S, Schreiner LJ, el-Khatib E. Factors influencing lung density in experimental models: results of studies using CT densitometry. *Physiol Meas*. 1993;14:183–193.
28. Carson RE. Parameter estimation in positron emission tomography. In: Phelps ME, Mazziotta J, Schelbert HR, eds. *Positron Emission Tomography and Autoradiography: Principles and Applications for the Brain and Heart*. New York, NY: Raven Press; 1986:347–390.
29. Tjuvajev JG, Avril N, Oku T, et al. Imaging herpes virus thymidine kinase gene transfer and expression by positron emission tomography. *Cancer Res*. 1998;58:4333–4341.
30. de Vries EF, van Dillen IJ, van Waarde A, et al. Evaluation of [<sup>18</sup>F]FHPG as PET tracer for HSVtk gene expression. *Nucl Med Biol*. 2003;30:651–660.
31. Liang Q, Nguyen K, Satyamurthy N, et al. Monitoring adenoviral DNA delivery, using a mutant herpes simplex virus type 1 thymidine kinase gene as a PET reporter gene. *Gene Ther*. 2002;9:1659–1666.
32. Dreyfuss D, Soler P, Saumon G. Mechanical ventilation-induced pulmonary edema: interaction with previous lung alterations. *Am J Respir Crit Care Med*. 1995;151:1568–1575.
33. Cunningham AL, Hurley JV. Alpha-naphthyl-thiourea-induced pulmonary edema in the rat: a topographical and electron-microscope study. *J Pathol*. 1972;106:25–35.
34. Minty BD, Scudder CM, Grantham CJ, Jones JG, Bakhle YS. Sequential changes in lung metabolism, permeability, and edema after ANTU. *J Appl Physiol*. 1987;62:491–496.
35. Doubrovin M, Ponomarev V, Beresten T, et al. Imaging transcriptional regulation of p53-dependent genes with positron emission tomography in vivo. *Proc Natl Acad Sci USA*. 2001;98:9300–9305.
36. Green L, Yap C, Nguyen K, et al. Indirect monitoring of endogenous gene expression by positron emission tomography (PET) imaging of reporter gene expression in transgenic mice. *Mol Imaging Biol*. 2002;4:71–81.
37. Richard JC, Factor P, Welch LC, Schuster DP. Imaging the spatial distribution of transgene expression in the lungs with positron emission tomography. *Gene Ther*. 2003;10:2074–2080.

